



# 755 nm InP/GaAs<sub>0.65</sub>P<sub>0.35</sub> quantum dot laser with polarization-dependent emission from type-I and type-II band alignments

WEN GU,<sup>†</sup>  BOQUN ZHAO,<sup>†</sup> YING XUE,<sup>†</sup>  AND KEI MAY LAU<sup>\*</sup> 

*Division of Emerging Interdisciplinary Area, Hong Kong University of Science and Technology, Clear Water Bay, Kowloon, Hong Kong SAR, China*

<sup>†</sup>These authors contributed equally.

<sup>\*</sup>[ekmlau@ust.hk](mailto:ekmlau@ust.hk)

**Abstract:** InP/GaAs<sub>0.65</sub>P<sub>0.35</sub> quantum dot (QD) lasers with variable polarization are demonstrated through the tailoring of band alignment. Different band alignments of type-I and type-II are realized during QD growth with varied parameters. The energy shift of type-I structure is observed to be much lower than that of type-II. Furthermore, type-I and type-II band ridge waveguide lasers were investigated. For type-I and type-II band lasers, the lowest thresholds are 0.37 and 0.40 kA/cm<sup>2</sup>, respectively, and different polarization characteristics are achieved. We observed transverse electric (TE) and transverse magnetic (TM) polarized light resulted from different band alignments, and the degree of polarization (DOP) reached 80%. These results indicate that InP/GaAs<sub>0.65</sub>P<sub>0.35</sub> QDs can be potentially used in devices with desired polarization.

© 2025 Optica Publishing Group under the terms of the [Optica Open Access Publishing Agreement](#)

## 1. Introduction

Self-assembled semiconductor quantum dots (QDs) have attracted significant interest in optoelectronic device applications, including lasers [1,2], light-emitting diodes [3], and photodetectors [4,5]. The polarization properties of the QD lasers are crucial due to their great influence on device performance. For example, both transverse electric (TE) and transverse magnetic (TM) polarized QD gains are desired to reduce the polarization fluctuations of output signal in polarization-insensitive semiconductor optical amplifiers (SOAs). Compared with the mature TE-polarized QD lasers, the development of TM-polarized QD lasers is not straightforward due to the low aspect ratio and naturally compressive strain in QDs [6]. Considerable efforts have been made to enhance the TM component in QD lasers, such as the control of QD shape or size [7], aspect ratio [8], and multi-stacking [9]. Another approach to improving the TM component is the modification of the band alignment. For example, TE/TM polarization switching has been observed in type-I and type-II band InGaAs QDs capped by GaAsSb [10]. Up to now, TM-polarized InAs QD lasers at 1.5 μm have been realized in optical communication systems [11,12]. InP QDs, compared with their InAs QD counterparts, are also desired in high-speed and low-cost devices for bio-sensing and biomedical applications [13]. However, TM-polarized InP QDs leading to the development of polarization-insensitive devices have not been reported. Initial studies have proved that InP QDs embedded in AlGaInP quantum well (QW) structures can yield both type-I and type-II band alignments [7,14]. For example, the band alignment of InP/GaInP QD heterostructures can be changed from type-I to type-II with the increase of QD size [15]. Besides, type-II band alignment for InP/GaAs QDs has also been demonstrated by photoluminescence (PL) measurement and surface photovoltage spectroscopy [16,17]. However, few studies have focused on the effects of band alignment on InP QD laser performance, particularly with regard to polarization properties. In previous work, GaAsP QWs have been demonstrated to act as the strain layer to grow InP QDs [18]. The adoption of embedded InP QDs in tensile-strained GaAsP QWs should affect the polarization of laser due to the modification of the band alignment.

In this work, TE- and TM-polarized InP/GaAs<sub>0.65</sub>P<sub>0.35</sub> QD lasers are reported using type-I and type-II band structures. The effects of growth parameters, specifically the V/III ratio, on the micro-photoluminescence ( $\mu$ -PL) performance of InP QD structures were first investigated to confirm the band alignments. Subsequently, electrically pumped InP/GaAs<sub>0.65</sub>P<sub>0.35</sub> QD ridge waveguide lasers were fabricated. The type-I and type-II band lasers are determined to be TE- and TM-polarized, respectively, with the same degree of polarization (DOP) of around 80%.

## 2. Materials growth and structure design

The epitaxial structures were grown on semi-insulating GaAs (100) substrates in a low-pressure metal-organic chemical vapor deposition (MOCVD) system (AIXTRON 200/4). Four samples were grown for this study: single Al<sub>0.4</sub>Ga<sub>0.6</sub>As/GaAs<sub>0.65</sub>P<sub>0.35</sub> quantum well (SQW, sample A), single layer quantum dots (SQDs, samples B and C) in QW (DWELL), and triple layer quantum dots (3-layer QDs, sample D). Before growth, substrates were treated using high temperature annealing to remove native oxide. Figure 1 depicts the schematic of sample structures. The growth of sample A started with a 100-nm GaAs buffer at 650 °C, followed by an 8-nm tensile-strained GaAs<sub>0.65</sub>P<sub>0.35</sub> QW sandwiched by two 70-nm Al<sub>0.4</sub>Ga<sub>0.6</sub>As barriers. For samples B and C, the DWELL structure was formed by inserting InP QDs in the middle of the GaAs<sub>0.65</sub>P<sub>0.35</sub> QW through the Stranski-Krastanov (SK) growth mode. The growth parameters of the GaAs<sub>0.65</sub>P<sub>0.35</sub> QW for samples B and C were kept the same as sample A. The InP QDs were grown at 680 °C, with a growth rate of 0.2 ML/s, a growth time of 16 s, and a growth interruption time of 3 mins. The V/III ratios for samples B and C were 5.5 and 32, respectively, to investigate the effect of the V/III ratio on the QD properties. For sample D, the active region was repeated three times based on sample C, with each cycle separated by a 20-nm Al<sub>0.4</sub>Ga<sub>0.6</sub>As barrier. In addition, for all the InP QD samples, an extra layer of InP QDs was grown on the top surface in order to characterize the morphology of the QDs. After that, electrically pumped ridge waveguide laser structures based on samples B and D were grown to explore the impacts of QD growth conditions on the laser performance. The growth sequence of the laser structures was as follows: 700-nm n-GaAs contact layer ([Si]:  $1 \times 10^{19} \text{ cm}^{-3}$ ), 750-nm n-type Al<sub>0.7</sub>Ga<sub>0.3</sub>As cladding layer ([Si]:  $2.6 \times 10^{17} \text{ cm}^{-3}$ ), QD active region (same as samples B and D), 750-nm p-type Al<sub>0.7</sub>Ga<sub>0.3</sub>As cladding layer ([Zn]:  $1.6 \times 10^{18} \text{ cm}^{-3}$ ), and 230-nm p-type GaAs contacting layer ([Zn]:  $4.6 \times 10^{19} \text{ cm}^{-3}$ ).

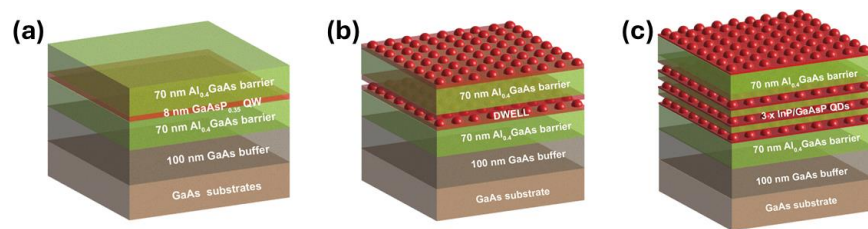


Fig. 1. Schematic of the as-grown (a) SQW, (b) SQDs, and (c) 3-layer QD structures.

## 3. Results and discussion

### 3.1. Materials characterization

The morphology of all the samples was characterized using atomic force microscope (AFM), as shown in Fig. 2. A smooth surface over  $10 \mu\text{m} \times 10 \mu\text{m}$  areas with a roughness of 0.1 nm is observed for sample A with single QW. For the QD samples, it was found that only nucleation layers form when the V/III ratio is lower than 3.5 (data not shown). A quantum dash (QDash)

morphology is observed when grown with a V/III ratio of 5.5, evolving to QD morphology as the V/III ratio was increased, as shown in Figs. 2(b)-(c). This transition is attributed to the increased migration of indium atoms at higher V/III. The average height of the QD or QDash ranges from 4 to 7 nm, and no significant non-uniformity was observed. Figure 2(d) shows the morphology of the 3-layer QD sample. Some clusters form randomly owing to the coalescence of QDs under larger accumulated strain. The approximated densities of QDash or QD for samples B, C, and D are  $1.6$ ,  $2.2$ , and  $1.8 \times 10^{10} \text{ cm}^{-2}$ , respectively. In the literature, only InP QDs have been reported in conventional InP/AlGaInP QD systems [19,20], and the InP QDash morphology is observed here and compared with QDs in the InP/GaAs<sub>0.65</sub>P<sub>0.35</sub> system.

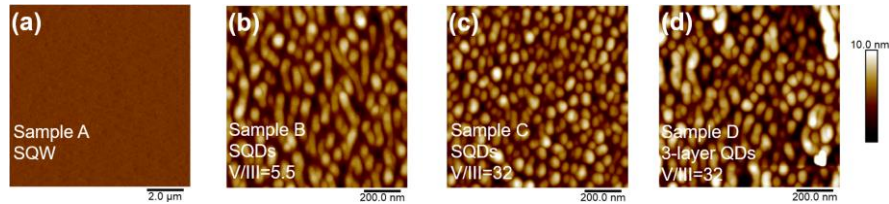


**Fig. 2.** (a)  $10 \mu\text{m} \times 10 \mu\text{m}$  AFM image of sample A;  $1 \mu\text{m} \times 1 \mu\text{m}$  AFM images of (b) sample B, (c) sample C and (d) sample D.

To investigate the band alignment characteristics, all samples were pumped by a 532-nm continuous-wave (CW) diode laser for room temperature (RT) power-dependent  $\mu$ -PL measurements. Figures 3(a)-(d) show the normalized PL spectra of samples A to D as the excitation power density increases from 4 to  $800 \text{ W/cm}^2$ . For sample A, two peaks located at 690 and 715 nm are observed, attributed to the heavy hole (HH) and light hole (LH) bands in the tensile-strained GaAs<sub>0.65</sub>P<sub>0.35</sub> QW structures [21]. For sample B, the PL peak is located at around 750 nm and shifts a little, while apparent blue shifts of PL peaks are observed for samples C and D.

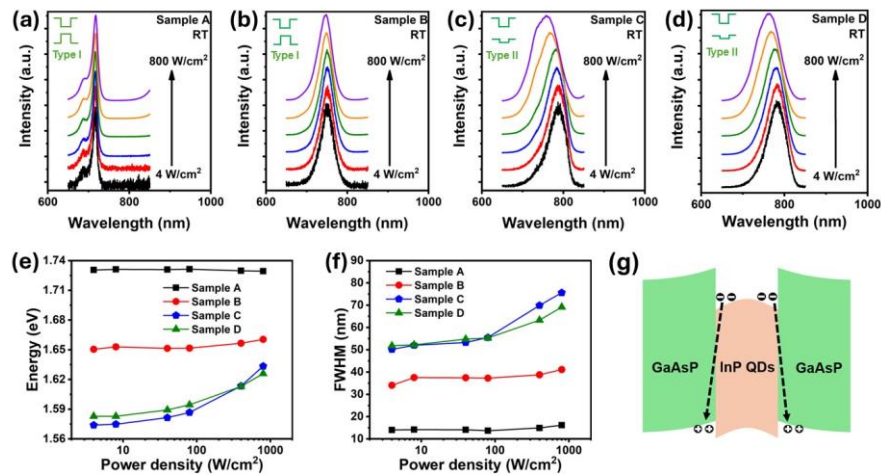


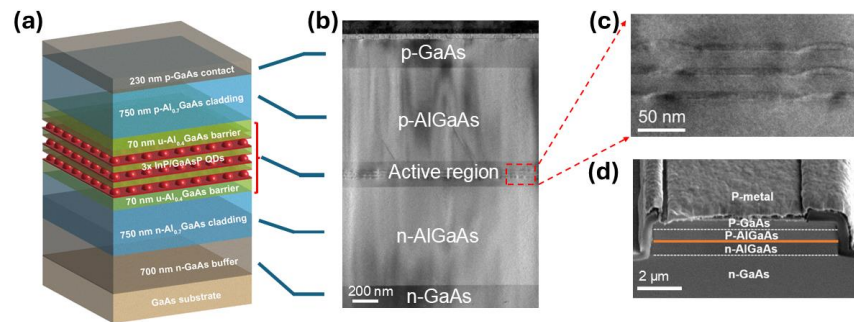
**Fig. 3.** Power-dependent  $\mu$ -PL spectra of (a) sample A, (b) sample B, (c) sample C, and (d) sample D; (e) Energy and (f) FWHM shifts of sample A to D along with the increase of excitation power density; (g) Schematic of the band bending effect in the type-II InP/GaAs<sub>0.65</sub>P<sub>0.35</sub> QDs.

For better observation, the shifts in PL energy and full width at half maximum (FWHM) for samples A to D with increasing excitation power density are shown in Figs. 3(e)-(f). For sample A, the PL energy shifts 2 meV with increasing excitation power density, indicating a typical type-I

band structure for the  $\text{GaAs}_{0.65}\text{P}_{0.35}/\text{Al}_{0.4}\text{Ga}_{0.6}\text{As}$  SQW [22]. For sample B, an energy shift of 10 meV to higher energy is observed due to state filling in the QDs. This small energy shift is similar to the reported value of 10~20 meV for type-I band InP/GaP QDs [23], suggesting that sample B also has a type-I structure. For samples C and D, greater blue shifts of 60 and 43 meV are observed. These values are larger than that of the reported value of 35 meV with a wider range of excitation power density for type-II band InP/GaInP structures [24]. Thus, samples C and D are mostly type-II band structures. Besides, compared with the type-I band structures (samples A and B), the type-II band structures (samples C and D) also exhibit more significant FWHM variations. Figure 3(g) shows the band bending effect for the type-II band InP/GaAs<sub>0.65</sub>P<sub>0.35</sub> embedded QDs, which can be used to explain the large blue shift at high excitation power density. In the type-II structures, a strong electric field at the interface is induced by the spatially separated carriers, leading to the conduction and valence band bending. As the excitation power density increases, the band bending is pronounced, giving rise to a narrower region to confine carriers. As a result, the quantized energy for carriers is enlarged, resulting in a significant blue shift.

### 3.2. Device performance

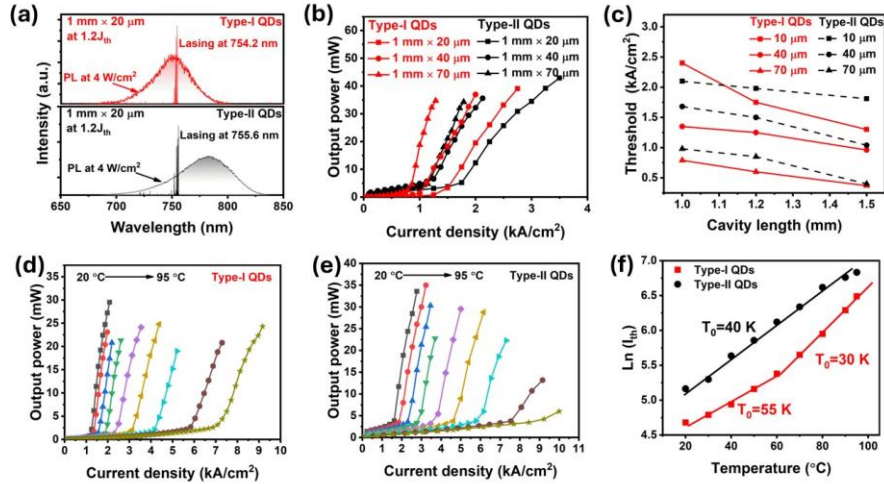
To investigate the impact of InP/GaAs<sub>0.65</sub>P<sub>0.35</sub> QD band alignment on the laser performance, ridge waveguide lasers were fabricated. The fabrication process was described in Ref. [25]. The electrically pumped type-II band 3-layer QD laser structure is shown in Fig. 4(a). Figure 4(b) shows the cross-sectional transmission electron microscope (TEM) image of the laser structure. The interface between the different layers can be clearly observed. A zoomed-in image of the active region, shown in Fig. 4(c), reveals the formation of the QDs. The 3-layer QDs align along with the growth direction with no obvious defects observed. The lateral size and height of each QD are around 70 and 10 nm, respectively. A 52°-tilted scanning electron microscope (SEM) image of the fabricated ridge waveguide laser is shown in Fig. 4(d). The end facet is mirror-like and smooth, ensuring low loss.



**Fig. 4.** (a) Schematic of the electrically pumped type-II bands QD laser; (b) Cross-sectional TEM image of the QD laser structure; (c) Zoom-in cross-sectional TEM image to observe the InP QDs; (d) 52°-tilted SEM image of the laser cavity.

The cleaved laser bars were placed on a heatsink with a temperature controller (limited to 95 °C max) and tested under pulsed conditions with a duty cycle of 0.5% and a pulse width of 400 ns. Figure 5(a) shows the representative RT lasing spectra at  $1.2J_{th}$  of the type-I and type-II band QD lasers with a cavity length of 1 mm and cavity width of 20 μm (referred to as 1 mm × 20 μm hereafter), superimposed with the PL spectra. Both lasers exhibit multimode emissions with a primary peak of around 755 nm. More than ten devices with different dimensions were measured for each sample, showing similar characteristics. The lasing wavelength for type-I band QD laser is between 750 to 766 nm, while the type-II band QD laser lase at 751 to 757 nm. Compared with the PL emissions at RT (at a power density of 4 W/cm<sup>2</sup>), the lasing wavelengths for the

type-I and type-II band QD lasers are red and blue shifted, which can be attributed to the heat accumulation in the active region, and the band filling and bending effect in type-II structures, respectively [26].



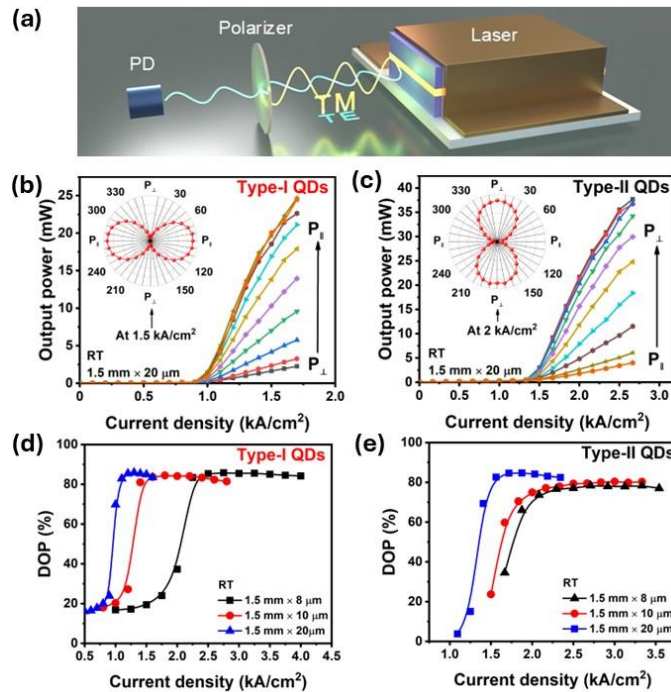
**Fig. 5.** (a) Lasing spectra of the type-I and type-II band QD laser at the current of  $1.2J_{th}$ ; (b) Representative L-I curves and (c) cavity length dependence on the threshold current density for the type-I and type-II band QD laser; Temperature dependence on the L-I curves of (d) type-I and (e) type-II band QD laser; (f) Characteristic temperatures of the type-I and type-II band QD laser.

Figure 5(b) shows representative light-current density (L-I) curves of the type-I and type-II band QD lasers with different device dimensions at RT. The threshold of the type-I band QD laser is somewhat lower than that of the type-II band QD laser. Figure 5(c) shows the cavity length dependence of the threshold current density for the type-I and type-II band lasers. The threshold current density decreases as the cavity length increases for both devices. The lowest threshold current density for the type-I and type-II band QD lasers are  $0.37$  and  $0.40$   $\text{kA/cm}^2$ , respectively, achieved with a device dimension of  $1.5 \text{ mm} \times 70 \mu\text{m}$ . It is worth noting that the type-I and type-II band QD lasers have different stackings, remarkably affecting the threshold as demonstrated in our previous work [18]. Additionally, in this study, the device based on the type-II band SQDs (sample C) was also fabricated. However, the yield of lasing devices was much lower, with only QW emission at  $725 \text{ nm}$  observed (not shown). This suggests that type-II band QD laser requires more stacking to improve QD gain compared with type-I band QD laser.

The temperature dependence of the L-I curves for type-I and type-II band QD lasers with a device dimension of  $1.2 \text{ mm} \times 10 \mu\text{m}$  is shown in Figs. 5(d) to (f). Both type-I and type-II band QD lasers can operate at temperatures up to  $95 \text{ }^\circ\text{C}$ . With the increase of operation temperatures from  $20$  to  $95 \text{ }^\circ\text{C}$ , the slope efficiency of the type-I band QD laser gradually reduces from  $0.42$  to  $0.13 \text{ W/A}$ . The slope efficiency of the type-II band QD laser decreases from  $0.26$  to  $0.15 \text{ W/A}$  at the operation temperature of  $20$  to  $80 \text{ }^\circ\text{C}$  and degrades noticeably to  $0.02 \text{ W/A}$  at  $95 \text{ }^\circ\text{C}$ . It is attributed to the higher internal quantum efficiency (IQE) in the type-I band structures. The characteristic temperatures ( $T_0$ ) extracted for type-I band QD laser is  $55 \text{ K}$  below  $60 \text{ }^\circ\text{C}$  and decreased to  $30 \text{ K}$  at  $60$  to  $95 \text{ }^\circ\text{C}$ , while a  $T_0$  of  $40 \text{ K}$  is obtained for type-II band QD laser. It indicates the inferior thermal stability for the type-I band QD laser at high temperatures, probably due to the lower stacking numbers.

The polarization characteristics of the type-I and type-II band QD lasers were investigated by measuring the relative output power intensities as a function of the polarizer rotation angle. A

polarizer was inserted between the laser and photodetector (PD), with the measurement setup shown in Fig. 6(a). The GaAs<sub>0.65</sub>P<sub>0.35</sub> SQW laser was first measured to calibrate the polarization angle of the polarizer for TE and TM light, aligned with P<sub>||</sub> and P<sub>⊥</sub>, respectively. For the type-I band QD laser with a device dimension of 1.5 mm × 20 μm, the output power increases as the polarizer is rotated from P<sub>⊥</sub> to P<sub>||</sub>, as shown in Fig. 6(b). The angular polar plot exhibits symmetry along the P<sub>||</sub> direction, and the maximum power density is achieved at P<sub>||</sub>, indicating TE polarization for the type-I band QD laser. For the type-II band QD laser with the same device dimension, an increase in output power is observed as the polarizer rotates from P<sub>||</sub> to P<sub>⊥</sub>, as shown in Fig. 6(c). The angular polar plot of the laser power peak intensities at 2 kA/cm<sup>2</sup> shows a twofold symmetry with the axis along the P<sub>⊥</sub> direction, as shown in the insert, indicating TM polarization for the type-II band QD laser.



**Fig. 6.** (a) Schematic of the polarization measurement setup; L-I curves of the (b) type-I and (c) type-II band QD lasers at progressively increased polarizer angle with the inserted angular polar plots of the polarized laser power peak intensities; DOP of the (d) type-I and (e) type-II band QD laser with different device dimensions.

The degree of polarization (DOP) is defined as  $(P_{||}-P_{\perp})/(P_{||}+P_{\perp})$  for the type-I band laser and  $(P_{\perp}-P_{||})/(P_{||}+P_{\perp})$  for the type-II band laser. As the current density increases, the DOP for both the type-I and type-II band lasers increases and saturates at around 80%. The DOP shows little dependence on the device dimensions, as shown in Figs. 6(d) and (e). In the type-I band QD laser, HH is confined in the compressively strained QDs, generating TE-polarized light. In the type-II band QD lasers, LH is confined in the tensile-strained GaAs<sub>0.65</sub>P<sub>0.35</sub> QW and participates in the optical transition to generate TM polarized light. These results suggest that the polarization properties of InP/GaAs<sub>0.65</sub>P<sub>0.35</sub> QDs can be tuned by band alignment, which could be useful in polarization-insensitive applications, such as SOAs.

#### 4. Conclusion

We have investigated the effect of the growth parameters on the power-dependent PL of InP/GaAs<sub>0.65</sub>P<sub>0.35</sub> QDs, leading to type-I and type-II band structures. For type-I band SQDs, the energy shift is less than 10 meV, while a value larger than 43 meV is obtained for type-II band QDs. Ridge waveguide lasers with type-I and type-II band QDs in the active region were fabricated. Both the type-I and type-II band QD lasers lase at 755 nm, with distinctively red and blue shifted wavelengths compared with the PL wavelengths. The type-I band QD laser exhibits a somewhat lower threshold of 0.37 kA/cm<sup>2</sup> compared with the type-II band QD laser. The polarization characteristics of both devices were measured. The type-I and type-II band QD lasers show TE- and TM-polarization with a DOP of 80%, implying the polarization of the InP QD laser can be adjusted by band alignment. These findings suggest that the InP QDs embedded in GaAs<sub>0.65</sub>P<sub>0.35</sub> QWs could be applied in designed polarization devices.

**Funding.** Innovation and Technology Fund (ITS/201/19FP).

**Acknowledgments.** The authors would like to thank Nanosystem Fabrication Facility (NFF) and the Material Characterization & Preparation Facility (MCPF) of HKUST for their technical support.

**Disclosures.** The authors declare no conflicts of interest.

**Data availability.** Data underlying the results presented in this paper are not publicly available at this time but may be obtained from the authors upon reasonable request.

#### References

1. S. Chen, W. Li, J. Wu, *et al.*, "Electrically pumped continuous-wave III-V quantum dot lasers on silicon," *Nat. Photonics* **10**(5), 307–311 (2016).
2. Y. Yu, S. Liu, C. M. Lee, *et al.*, "Telecom-band quantum dot technologies for long-distance quantum networks," *Nat. Nanotechnol.* **18**(12), 1389–1400 (2023).
3. F. Hatami, V. Lordi, J. S. Harris, *et al.*, "Red light-emitting diodes based on InP/GaP quantum dots," *J. Appl. Phys.* **97**(9), 096106 (2005).
4. A. V. Barve, S. J. Lee, S. K. Noh, *et al.*, "Review of current progress in quantum dot infrared photodetectors," *Laser & Photonics Reviews* **4**(6), 738–750 (2010).
5. E. T. Kim, A. Madhukar, Z. Ye, *et al.*, "High detectivity InAs quantum dot infrared photodetectors," *Appl. Phys. Lett.* **84**(17), 3277–3279 (2004).
6. L. Huang, Y. Yu, P. Tian, *et al.*, "Polarization-insensitive quantum-dot coupled quantum-well semiconductor optical amplifier," *Semicond. Sci. Technol.* **24**(1), 015009 (2009).
7. T. Tayagaki and T. Sugaya, "Type-II InP quantum dots in wide-bandgap InGaP host for intermediate-band solar cells," *Appl. Phys. Lett.* **108**(15), 153901 (2016).
8. P. Jayavel, H. Tanaka, T. Kita, *et al.*, "Control of optical polarization anisotropy in edge emitting luminescence of InAs/GaAs self-assembled quantum dots," *Appl. Phys. Lett.* **84**(11), 1820–1822 (2004).
9. T. Inoue, M. Asada, N. Yasuoka, *et al.*, "Polarization control of electroluminescence from vertically stacked InAs/GaAs quantum dots," *Appl. Phys. Lett.* **96**(21), 211906 (2010).
10. P. Klenovský, D. Hemzal, P. Steindl, *et al.*, "Polarization anisotropy of the emission from type-II quantum dots," *Phys. Rev. B* **92**(24), 241302 (2015).
11. N. Yasuoka, H. Ebe, K. Kawaguchi, *et al.*, "Polarization-insensitive quantum dot semiconductor optical amplifiers using strain-controlled columnar quantum dots," *J. Lightwave Technol.* **30**(1), 68–75 (2012).
12. T. Kaizu, T. Kakutani, K. Akahane, *et al.*, "Polarization-insensitive fiber-to-fiber gain of semiconductor optical amplifier using closely stacked InAs/GaAs quantum dots," *Jpn. J. Appl. Phys.* **59**(3), 032002 (2020).
13. A. Müller, S. Marschall, O. B. Jensen, *et al.*, "Diode laser based light sources for biomedical applications," *Laser & Photonics Reviews* **7**(5), 605–627 (2013).
14. P. Dhingra, S. Fan, Y. Sun, *et al.*, "InP quantum dots for dislocation-tolerant, visible light emitters on Si," *Appl. Phys. Lett.* **117**(18), 181102 (2020).
15. D. V. Lebedev, A. M. Mintairov, A. S. Vlasov, *et al.*, "Lasing via excited state of type A InP/GaInP quantum dots embedded in microdisks," *J. Appl. Phys.* **132**(17), 173106 (2022).
16. S. D. Singh, V. K. Dixit, S. Porwal, *et al.*, "Observation of electron confinement in InP/GaAs type-II ultrathin quantum wells," *Appl. Phys. Lett.* **97**(11), 111912 (2010).
17. T. Ivanov, V. Donchev, K. Germanova, *et al.*, "Optical properties of multi-layer type II InP/GaAs quantum dots studied by surface photovoltage spectroscopy," *J. Appl. Phys.* **110**(6), 064302 (2011).
18. W. Luo, L. Lin, J. Huang, *et al.*, "Electrically pumped InP/GaAsP quantum dot lasers grown on (001) Si emitting at 750 nm," *Opt. Express* **30**(22), 40750–40755 (2022).
19. P. Dhingra, P. Su, B. D. Li, *et al.*, "Low-threshold InP quantum dot and InGaP quantum well visible lasers on silicon (001)," *Optica* **8**(11), 1495–1500 (2021).

20. Z. Huang, M. Zimmer, S. Hepp, *et al.*, "Optical gain and lasing properties of InP/AlGaInP quantum-dot laser diode emitting at 660 nm," *IEEE J. Quantum Electron.* **55**(2), 1–7 (2019).
21. F. Agahi, K. M. Lau, H. K. Choi, *et al.*, "High-performance 770-nm AlGaAs-GaAsP tensile-strained quantum-well laser diodes," *IEEE Photon. Technol. Lett.* **7**(2), 140–143 (1995).
22. B. Wang, L. Zhou, S. Tan, *et al.*, "71% wall-plug efficiency from 780 nm-emitting laser diode with GaAsP quantum well," *Opt. Laser Technol.* **168**, 109867 (2024).
23. F. Hatami, W. T. Masselink, L. Schrottke, *et al.*, "InP quantum dots embedded in GaP: Optical properties and carrier dynamics," *Phys. Rev. B* **67**(8), 085306 (2003).
24. R. Rödel, A. Bauer, S. Kremling, *et al.*, "Density and size control of InP/GaInP quantum dots on GaAs substrate grown by gas source molecular beam epitaxy," *Nanotechnology* **23**(1), 015605 (2012).
25. Y. Xue, W. Luo, S. Zhu, *et al.*, "1.55  $\mu\text{m}$  electrically pumped continuous wave lasing of quantum dash lasers grown on silicon," *Opt. Express* **28**(12), 18172–18179 (2020).
26. M. Peter, R. Kiefer, F. Fuchs, *et al.*, "Light-emitting diodes and laser diodes based on a  $\text{Ga}_{1-x}\text{In}_x\text{As}/\text{GaAs}_{1-y}\text{Sb}_y$  type II superlattice on InP substrate," *Appl. Phys. Lett.* **74**(14), 1951–1953 (1999).